Electronic Supporting Information (ESI)

Cobalt Sulphide Microtube Array as Cathode in Photoelectrochemical Water Splitting with Photoanodes

Chia-Yu Lin,[‡] *Dirk Mersch, David A. Jefferson, and Erwin Reisner**

Christian Doppler Laboratory for Sustainable SynGas Chemistry, Department of Chemistry, University of Cambridge, Lensfield Road, Cambridge CB2 1EW, UK.

‡ Current address: Department of Chemical Engineering, National Cheng Kung University, 1 University Road, Tainan City 70101, Taiwan.

* Corresponding author: reisner@ch.cam.ac.uk

Contents

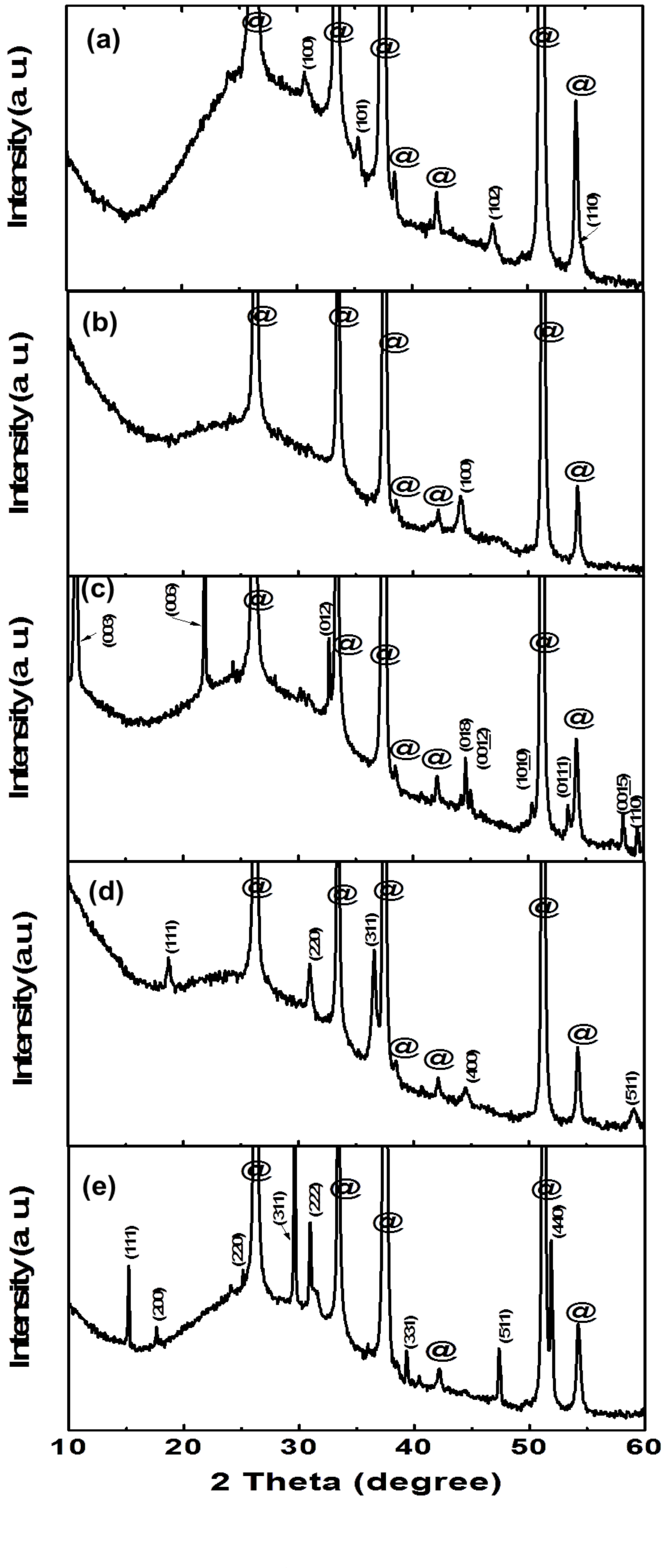

Figure S1. XRD patterns of (a) FTO|CoS, (b) FTO|Co, (c) FTO|Co(OH)$_2$, (d) FTO|Co$_3$O$_4$, and (e) FTO|Co$_9$S$_8$. The symbol @ shows the characteristic diffraction peaks of the FTO substrate and the corresponding Miller indices are also given. All cobalt species are identified by XRD (Figure S1a) with the corresponding JCPDS standard data (CoS, JCPDS card No. 75-0605; Co, JCPDS card No. 89-4307; Co$_3$O$_4$, JCPDS card No. 76-1802; Co$_9$S$_8$, JCPDS card No, 86-2273) or with reported literature[1] (α-Co(OH)$_2$).

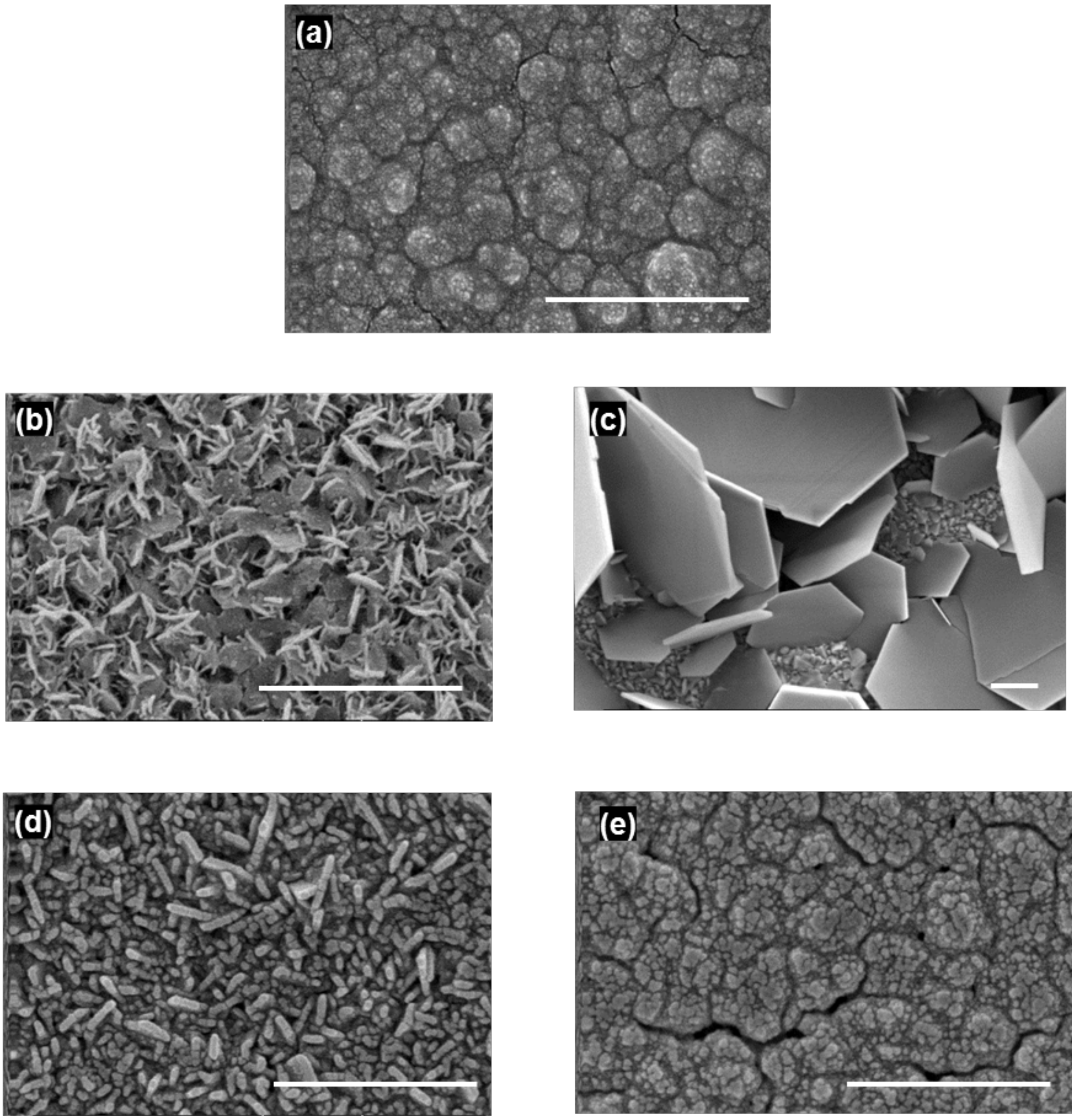

Figure S2. SEM images of (a) FTO|CoS, (b) FTO|Co, (c) FTO|Co(OH)$_2$, (d) FTO|Co$_3$O$_4$, and (e) FTO|Co$_9$S$_8$. Scale bar: 1 μm. The electrodeposited Co film (b) is composed of the nano-sized flakes and rather porous as compared with CoS film (a). The α-Co(OH)$_2$ film (c), on the other hand, is composed of micro-sized hexagonal platelets. Since all of the Co$_3$O$_4$ (d) and the Co$_9$S$_8$ (e) films are converted from the CoS film, the CoS, Co$_3$O$_4$ and Co$_9$S$_8$ show a dense morphology. In addition, due to the annealing process, the grain size of both films become larger as compared with the CoS film.

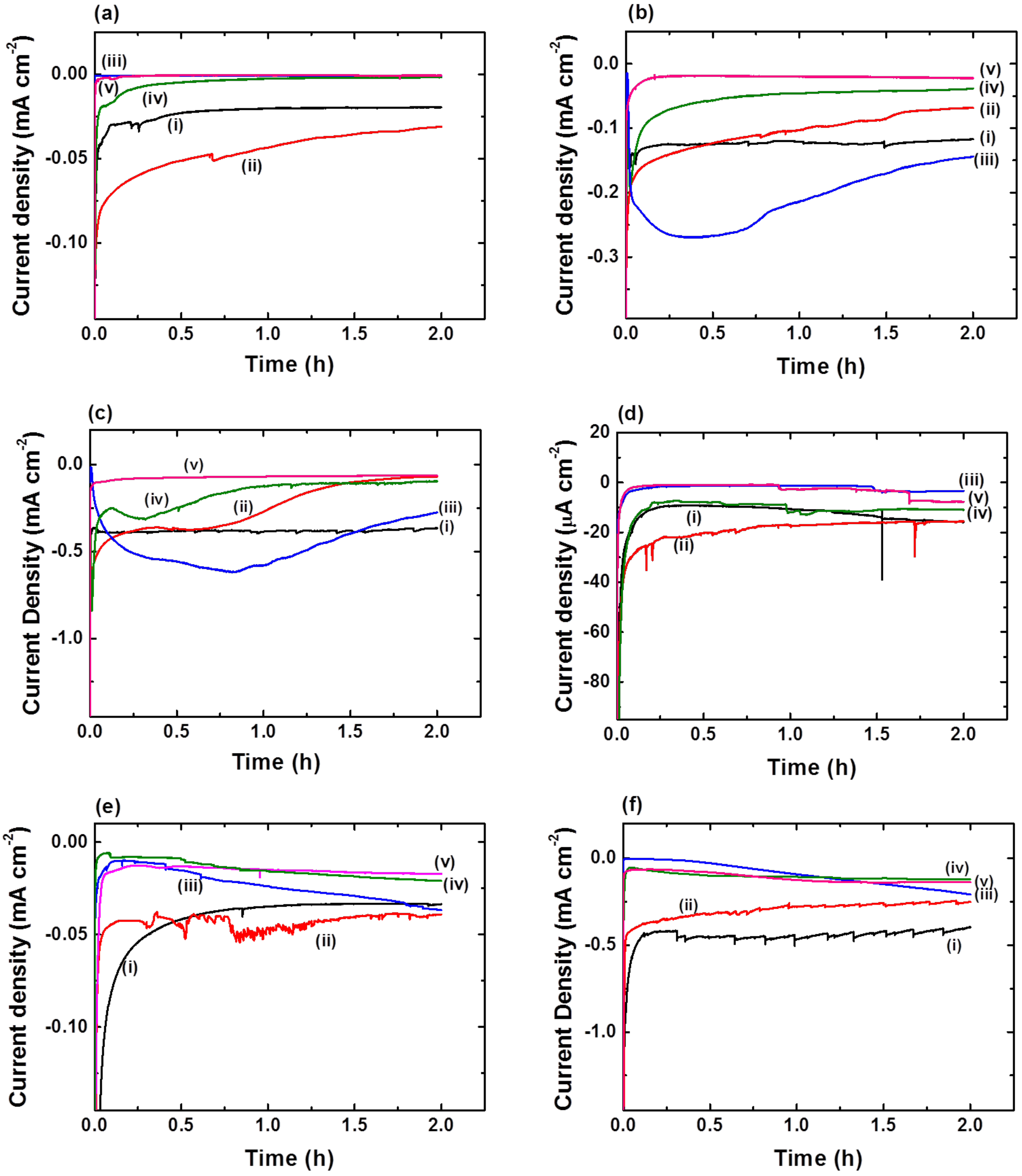

Figure S3. Chronoamperometric (I-t) curves for all Co species: (i) FTO|CoS, (ii) FTO|Co, (iii) FTO|Co(OH)$_2$, (iv) FTO|Co$_3$O$_4$, and (v) FTO|Co$_9$S$_8$ electrodes, in (a-c) pH 7 electrolyte solution containing TEOA (50 mM) and Na$_2$SO$_4$ (0.1 M) and (d-f) pH 13 electrolyte solution containing KOH (0.1 M) and Na$_2$SO$_4$ (0.1 M). The overpotential applied was 90 mV in a and d, 190 mV in b and e, and 290 mV in c and f.

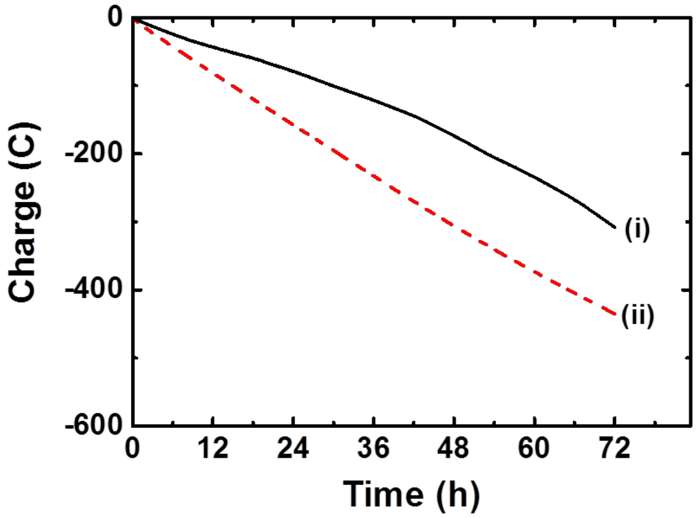

Figure S4. Charge transients of FTO|CoS at an overpotential of 390 mV (i) in pH neutral electrolyte solution containing TEOA (50 mM) and Na_2SO_4 (0.1 M), and (ii) in basic electrolyte solution containing KOH (0.1 M) and Na_2SO_4 (0.1 M).

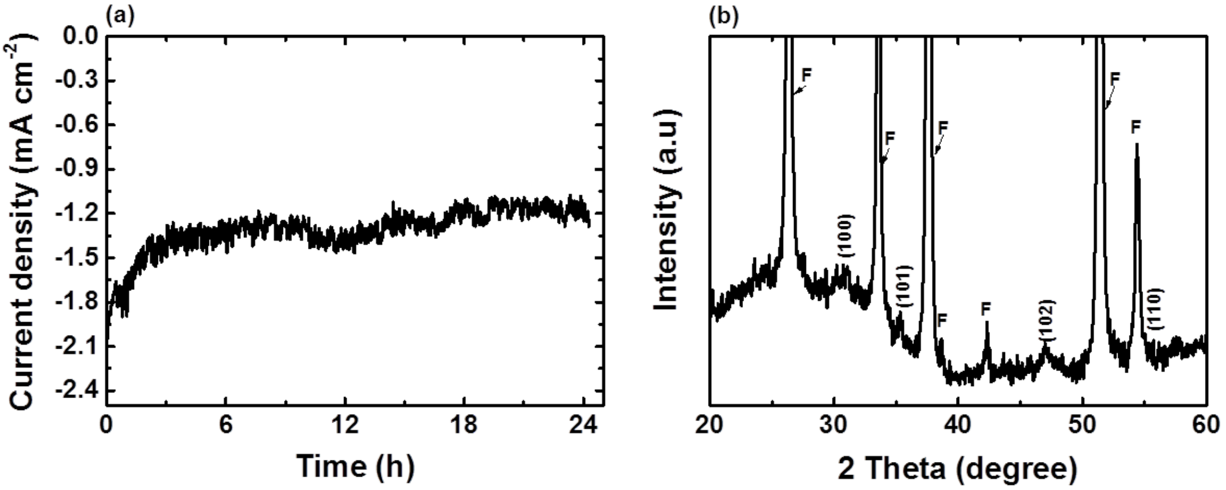

Figure S5. (a) Chronoamperometry of FTO|CoS at an overpotential of 390 mV in pH 7 TEOA (50 mM) and Na_2SO_4 (0.1 M) solution. The fluctuation in the i-t curve can be attributed to the bubbling of H_2 gas. (b) XRD pattern of FTO|CoS after 24-h electrolysis. The symbol F shows the characteristic diffraction peaks of the FTO substrate. The result indicates that FTO|CoS is stable during prolonged electrolysis in neutral electrolyte solution.

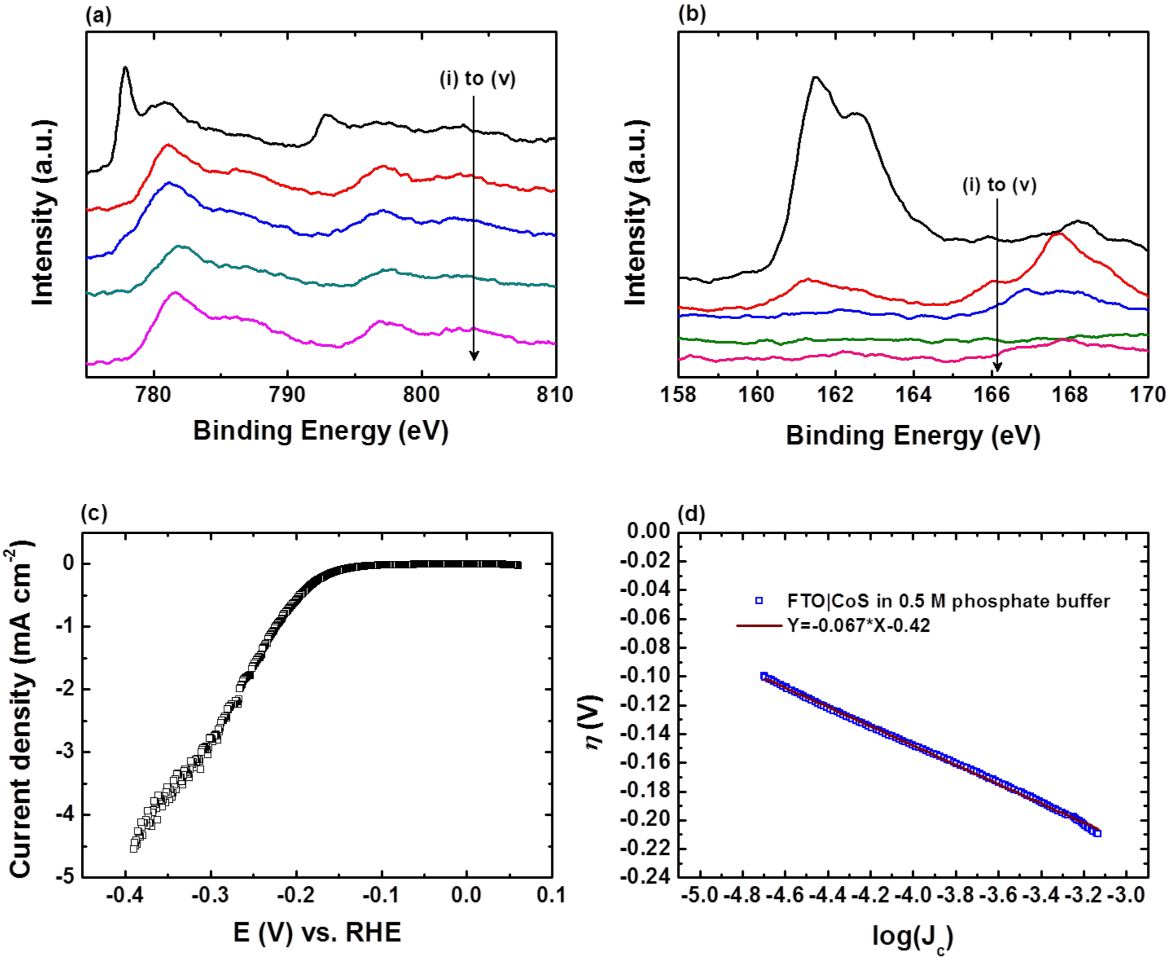

Figure S6. (a-b) XPS spectra of the FTO|CoS electrode (i) immersed in phosphate buffer (pH 7, 0.5 M), and after 2h controlled-potential electrolysis at (ii) η = 90 mV, (iii) η= 190 mV, (iv)η = 290 mV, (v) η = 390 mV in phosphate buffer (pH 7, 0.5 M). (a) Co 2p region. (b) S 2p region. (c) Linear sweep voltammetry and (d) the corresponding Tafel plots of the FTO|CoS electrode recorded at 0.05 mV s^{-1} in phosphate buffer (0.5 M, pH 7), where J_c is the cathodic current density. As revealed in this figure, we can see that the characteristic signals for CoS start to disappear even when the FTO|CoS was immersed in the buffer solution without applied potential, indicating CoS film is not stable in phosphate electrolyte solution. In addition, the Co $2p_{3/2}$ signal at binding energy of 781.5 eV rules out the possibility of formation of metallic cobalt. Furthermore, the P/Co/O ratio for the product after controlled-potential electrolysis at η =390 mV is 1:0.99:9.79. The decomposed CoS shows a Tafel slope of the decomposed CoS of 67 mV dec^{-1} and an overpotential of 220 mV is required to achieve current density of 1 mA cm^{-2} (c-d).

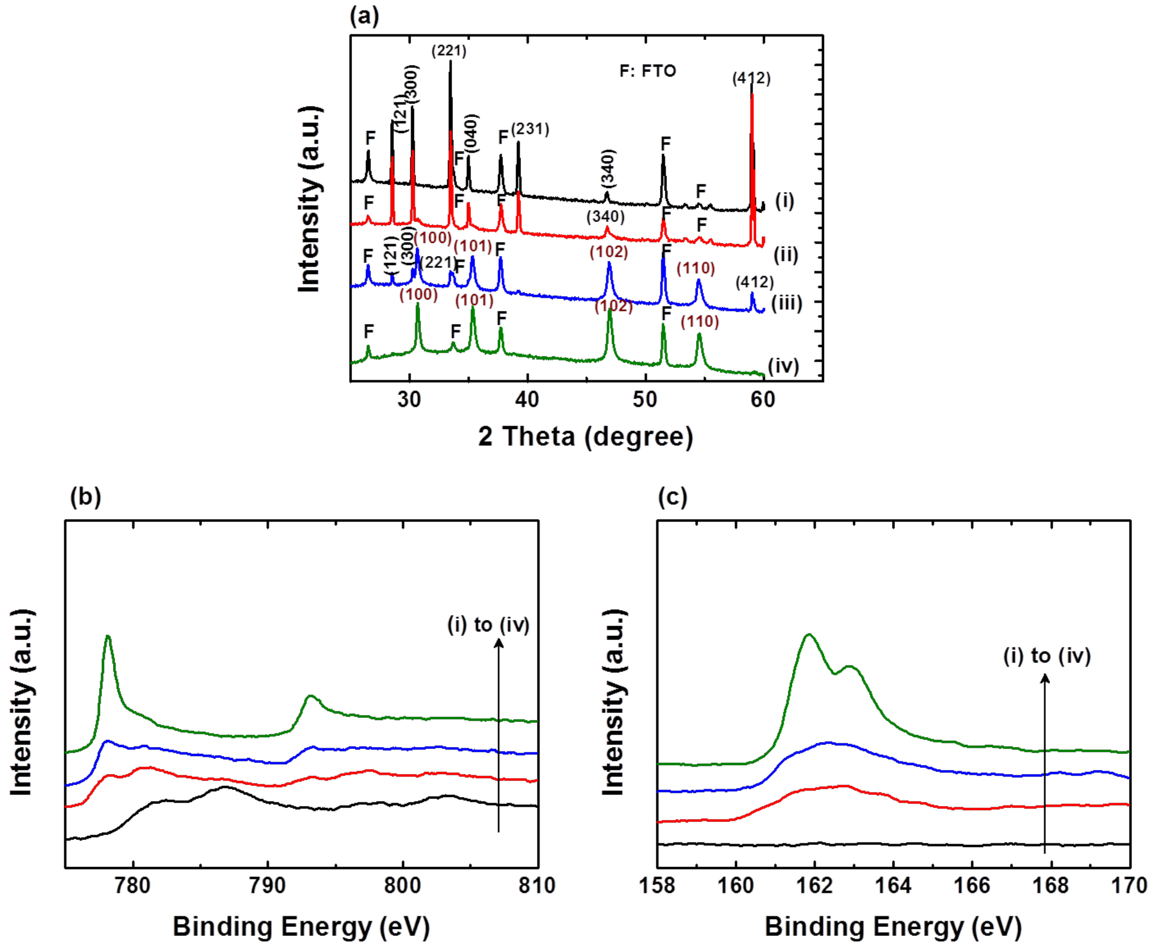

Figure S7. XRD and XPS of FTO|*nano*LHCC after CBD conversion for various time intervals. (a) XRD patterns and (b-c) XPS of FTO|*nano*LHCC after various CBD reaction times: (i) 0 h, (ii) 2 h, (ii) 4 h, and (iv) 6 h. (b) Co 2p region. (c) S 2p region. The symbol F shows the characteristic diffraction peaks of the FTO substrate and the Miller indices in black and in dark red show characteristic peaks of LHCC and CoS, respectively. Standard XRD data for *nano*LHCC and *micro*CoS are JCPDS card No. 48-0083 and JCPDS card No. 75-0605, respectively.

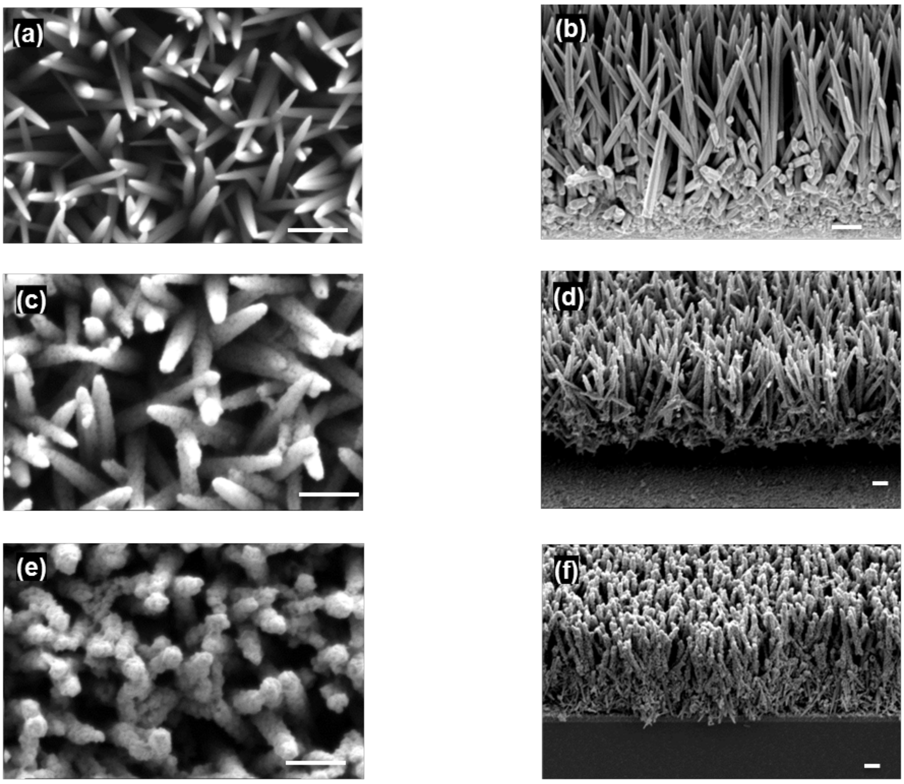

Figure S8. SEM images of FTO|*nano*LHCC after (a-b) 0-h, (c-d) 2-h, and (e-f) 4-h CBD sulphurisation. Scale bar: 1 μm.

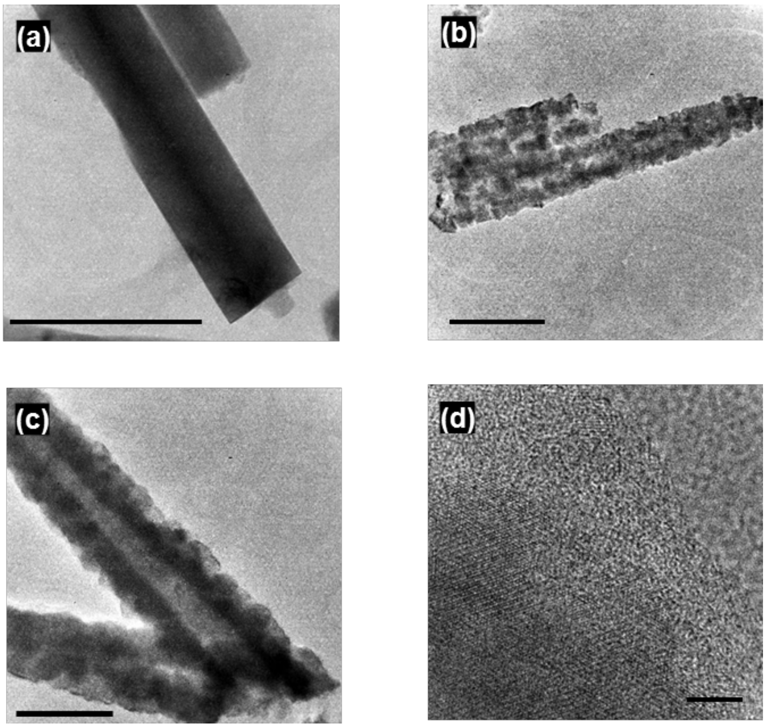

Figure S9. TEM images of (a) the as-prepared *nano*LHCC, and the *nano*LHCC after (b) 2-h and (c) 6-h CBD sulphurisation. (d) High resolution TEM image of *microCoS*. Scale bars in a-c and d present 500 nm and 5 nm, respectively.

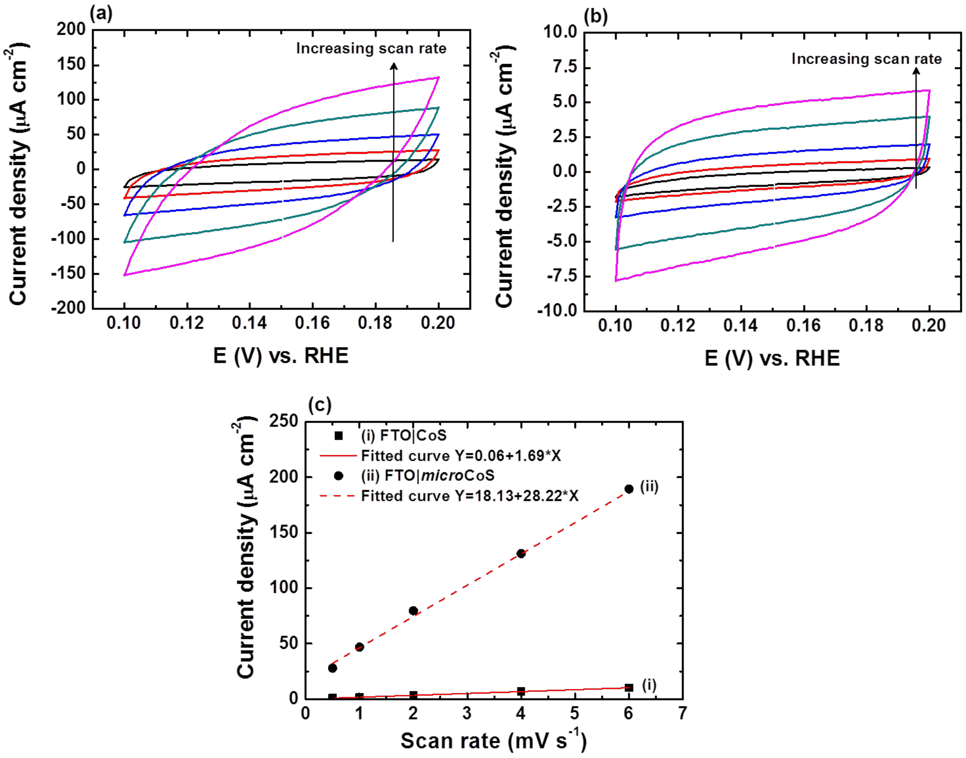

Figure S10. CVs of (a) FTO|*micro*CoS and (b) FTO|CoS electrodes recorded at various scan rates (ν), including 0.5, 1, 2, 4, and 6 mV s^{-1}, in TEOA buffer solution (50 mM, pH 7) containing Na_2SO_4 (0.1 M). The plots of △J *vs*. ν, where the △J is the sum of the anodic current and cathodic current measured at 0.15 V *vs*. RHE from (a) and (b), are shown in (c). The double layer capacitance (C_{dl}), determined using CV, can be used to estimate the effective surface area of the electrode-electrolyte solution interface.[2] (a-b) show the CVs of FTO|CoS and FTO|*micro*CoS electrodes at various scan rates (ν). It can be found that in the region of 0.1 to 0.2 V *vs*. RHE, the CV waves are square-like shape, indicating the currents are mostly resulted from the charge of the double layer. The capacitances of the CoS film and *micro*CoS were then estimated from the slope of the curve of charging current density *vs*. ν (c), where the slope is equal to $2C_{dl}$. However, since the area-averaged capacitance of the CoS is unknown, the relative effective surface area is calculated instead of actual effective surface area. As revealed in (c), the effective surface area of FTO|*micro*CoS is about 16.7 times higher than that of FTO|CoS.

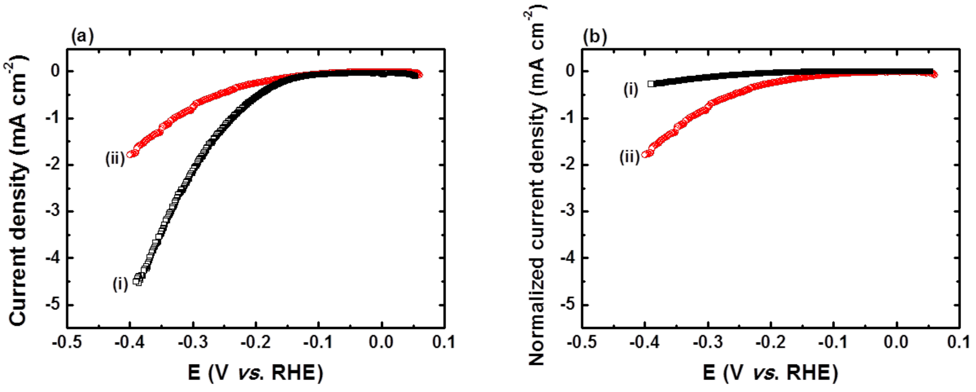

Figure S11. (a) Linear sweep voltammograms (LSVs), recorded at 0.05 mV s^{-1}, of (i) FTO|*micro*CoS (□) and (ii) FTO|CoS (○), in the basic electrolyte (pH 13) containing KOH (0.1 M) and Na_2SO_4 (0.1 M). Normalized LSVs with respect to the surface roughness (1 for FTO|CoS and 17 for FTO|*micro*CoS) are shown in (b).

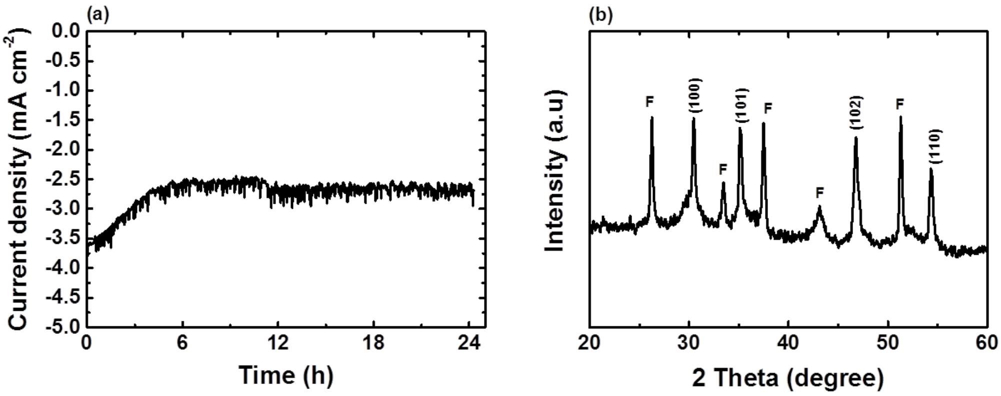

Figure S12. (a) Chronoamperometry of FTO|*micro*CoS at an overpotential of 390 mV in pH 7 TEOA (50 mM) and Na_2SO_4 (0.1 M) solution. The fluctuation in the i-t curve can be attributed to the bubbling of H_2 gas. (b) XRD pattern of FTO|*micro*CoS after 24-h electrolysis. The symbol F shows the characteristic diffraction peaks of the FTO substrate. The result indicates that FTO|*micro*CoS is stable during prolonged electrolysis in neutral electrolyte solution.

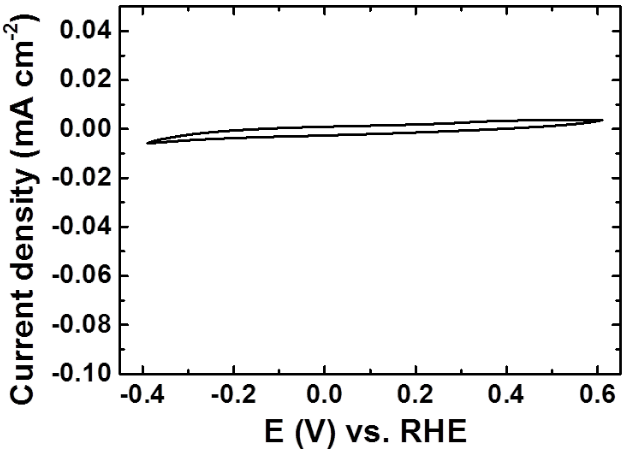

Figure S13. Cyclic voltammogram of FTO|*nano*LHCC recorded in pH 7 TEOA (50 mM) and Na_2SO_4 (0.1 M) solution at a scan rate of 50 mV s^{-1}.

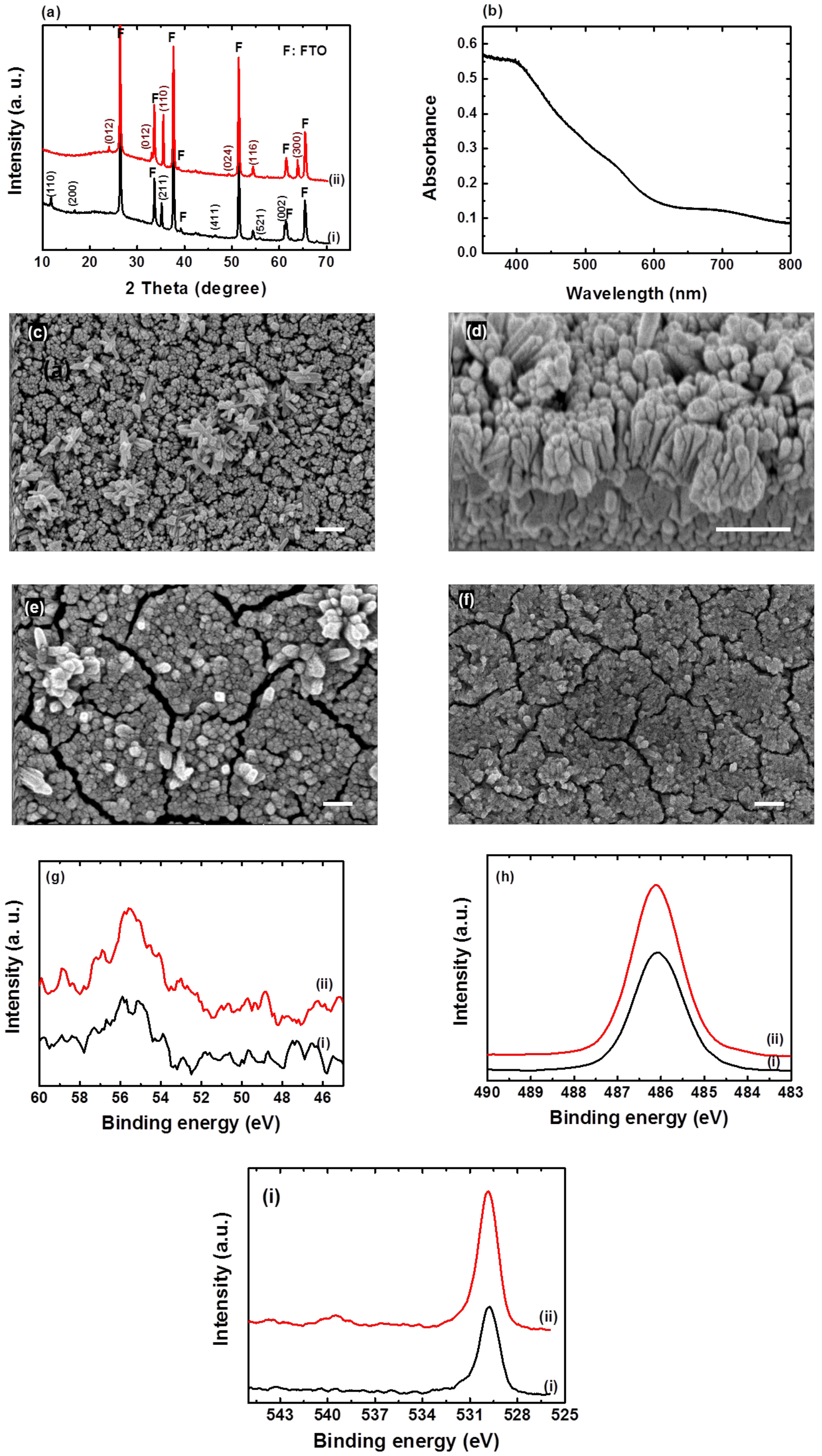

Figure S14. (a) XRD of (i) FTO|*nano*FeOOH and (ii) FTO|*nano*Fe_2O_3. The symbol F shows the characteristic diffraction peaks of the FTO substrate, whereas the Miller indices in black and in dark red depict characteristic peaks of β-FeOOH and α-Fe_2O_3, respectively. (b) UV-vis spectrum of FTO|*nano*Fe_2O_3. SEM images, with scale bar of 0.5 μm, of (c-d) FTO|*nano*FeOOH, (e) FTO|*nano*Fe_2O_3, and (f) FTO|*nano*Fe_2O_3 after the PEC experiment in Fig. 4c. (g-i) XPS data of FTO|*nano*Fe_2O_3 (i) before and (ii) after the PEC experiment in Fig. 4c; (g) Fe 3p region, (h) Sn 3d region, and (i) O 1s region. The peaks in Fe 3p (at 55.6 eV in g), Sn 3d (460.1 eV in h), and O 1s (530 eV in i) confirm that Sn is incorporated into the FeO structure,[3,4] and the minimal change in binding energy for all peaks indicate that the change in chemical composition of the FTO|*nano*Fe_2O_3 photoanode during the PEC experiments is minimal.

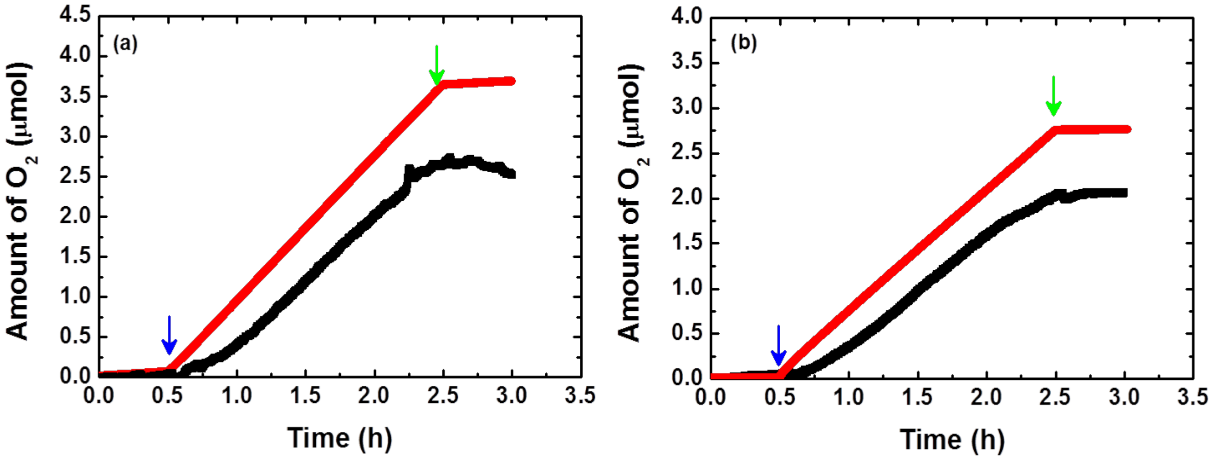

Figure S15. O_2 evolution during PEC water splitting with a two-electrode cell using a FTO|*nano*Fe_2O_3 photoanode and (a) Pt or (b) FTO|*micro*CoS as cathode in the electrolyte containing KOH (0.1 M) and Na_2SO_4 (0.1 M) at pH 13. An external bias of 1.23 V was applied throughout the experiment, but standardized solar light only applied between 0.5 and 2.5 h (blue and green arrows indicate the beginning and the end of PEC water splitting, respectively). The amount of O_2 was quantified by an O_2 fluorescence probe (black trace) and the theoretical amount of O_2 with 100% Faradaic efficiency is shown as the red trace.

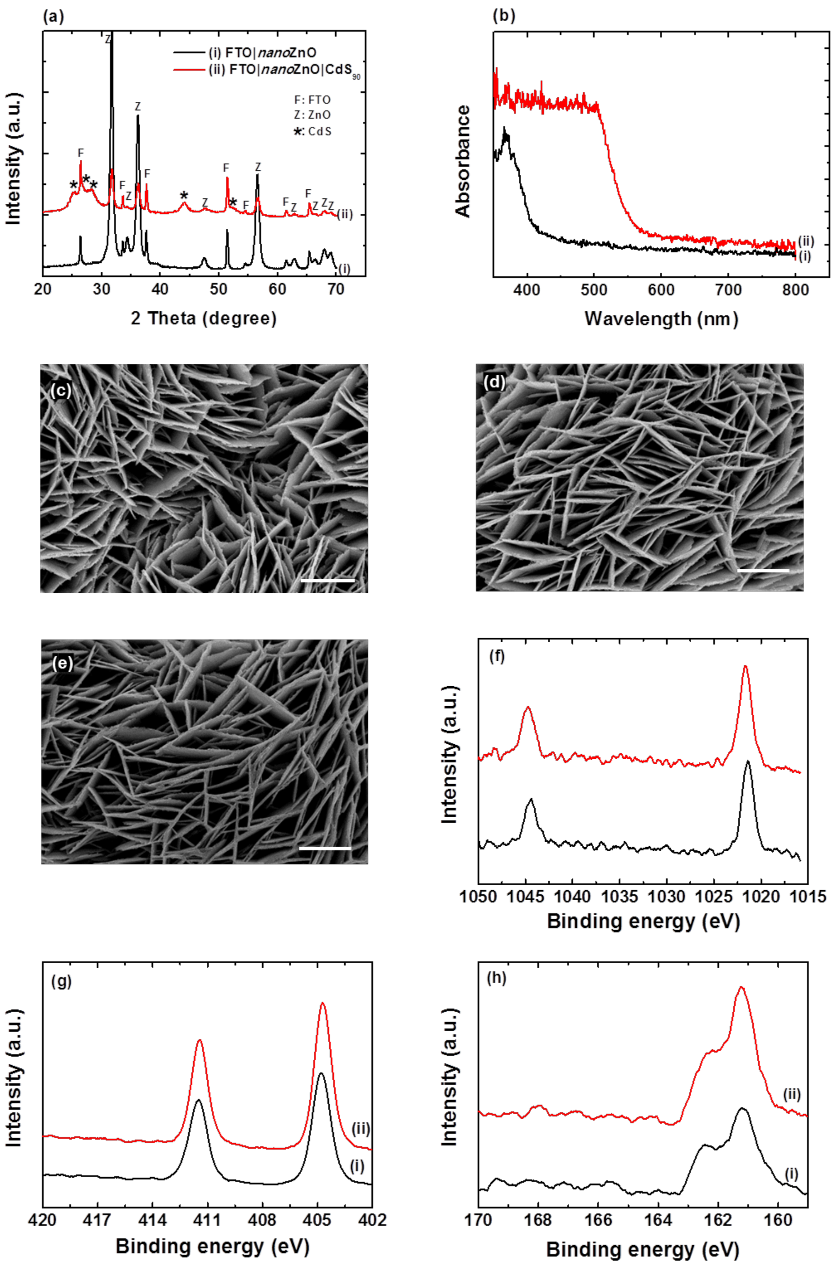

Figure S16. (a) XRD patterns, and (b) UV-vis spectra of (i) FTO|*nano*ZnO and (ii) FTO|*nano*ZnO|CdS$_{NP}$. Top-view SEM images, with scale bar of 2 μm, of (c) FTO|*nano*ZnO, (d) FTO|*nano*ZnO|CdS$_{NP}$, and (e) FTO|*nano*ZnO|CdS$_{NP}$ after the PEC experiment in Fig. 4d. (f-h) XPS data of FTO|*nano*ZnO|CdS$_{NP}$ (i) before and (ii) after PEC experiment in Fig. 4d; (f) Zn 2p region, (g) Cd 3d and (h) S 2p region. Hexagonal wurtzite-type CdS$_{NP}$ (JCPDS card No. 41-1049), with crystallite size of 10.2 nm calculated using XRD results (a) and the Scherrer equation, were deposited onto FTO|*nano*ZnO via CBD at room temperature for 90 min. As demonstrated by Spoerke *et al.*,[5] CdS$_{NP}$ can be selectively deposited onto the ZnO surface via the reaction between thioacetamide and cadmium hydroxide complex surface-bound on ZnO. Therefore, it is expected that when a uniform CdS$_{NP}$ layer is deposited on the *nano*ZnO surface, there is no change in microscopic surface morphology of FTO|*nano*ZnO (see Figs. c-d). No obvious change in the surface morphology was observed for of FTO|*nano*ZnO|CdS$_{NP}$, indicating that the nano-architecture of the photoelectrode is stable under PEC conditions. The UV-vis spectra in (b) show that the light absorption of the photoanode is extended to 575 nm after the CdS sensitisation. The apparent band gap, estimated from the onset of the absorption curves) of the FTO|*nano*ZnO|CdS$_{NP}$ photoanode is about 2.15 eV, which is smaller than that for the bulk CdS (2.4 eV),[6] which can be attributed to the light scattering induced by the 2-D nanostructure of *nano*ZnO. The XPS peaks in Zn 2p (at 1021.6 eV and 1044.6 in f), Cd 3d (104.28 eV and 411.4 eV in g), and S2p (161.2 eV and 162.3 eV in h) confirm that the formation of CdS$_{NP}$ on *nano*ZnO,[7] and the minimal change in binding energy for all peaks indicate that the change in chemical composition of FTO|*nano*ZnO|CdS$_{NP}$ photoanode during the PEC experiments is minimal.

References

1. Z. P. Liu, R. Z. Ma, M. Osada, K. Takada, T. Sasaki, *J. Am. Chem. Soc.*, 2005, **127**, 13869-13874.
2. S. Trasatti, O. A. Petrii, *Pure Appl. Chem.*, 1991, **63**, 711-734.
3. L. Xi, S. T. Chiam, W. F. Mak, P. D. Tran, J. Barber, S. C. J. Loo, L. H. Wong, *Chem. Sci.*, 2013, **4**, 164-169.
4. T. Yamashita, P. Hayes, *Appl. Surf. Sci.*, 2008, **254**, 2441-2449.
5. E. D. Spoerke, M. T. Lloyd, Y.-j. Lee, T. N. Lambert, B. B. McKenzie, Y.-B. Jiang, D. C. Olson, T. L. Sounart, J. W. P. Hsu, J. A. Voigt, *J. Phys. Chem. C*, 2009, **113**, 16329-16336.
6. Y. Myung, D. M. Jang, T. K. Sung, Y. J. Sohn, G. B. Jung, Y. J. Cho, H. S. Kim, J. Park, *ACS Nano*, 2010, **4**, 3789-3800.
7. K. Yuan, L. Chen, F. Li, Y. Chen, *J. Mater. Chem. C*, 2014, **2**, 1018-1027.